THE JOURNAL OF PHYSICAL CHEMISTRY B

Article

pubs.acs.org/JPCB

Fluorescence Properties of the Chromophore-Binding Domain of Bacteriophytochrome from *Deinococcus radiodurans*

Heli Lehtivuori,[†] Ilona Rissanen,[†] Heikki Takala,[†] Jaana Bamford,[†] Nikolai V. Tkachenko,[‡] and Janne A. Ihalainen*[,†]

[†]Nanoscience Center, Department of Biological and Environmental Science, University of Jyväskylä, P.O. Box 35, 40014 Jyväskylä, Finland

[‡]Department of Chemistry and Bioengineering, Tampere University of Technology, P.O. Box 541, 33101 Tampere, Finland

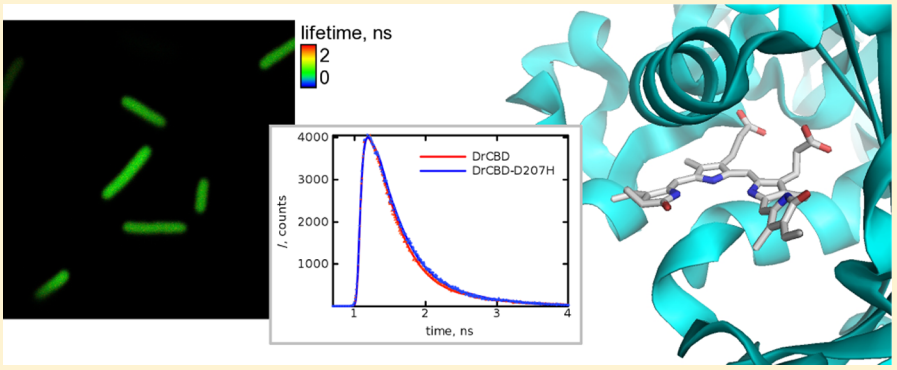

ABSTRACT: Fluorescent proteins are versatile tools for molecular imaging. In this study, we report a detailed analysis of the absorption and fluorescence properties of the chromophore-binding domain from *Deinococcus radiodurans* and its D207H mutant. Using single photon counting and transient absorption techniques, the average excited state lifetime of both studied systems was about 370 ps. The D207H mutation slightly changed the excited state decay profile but did not have a considerable effect on the average decay time of the system or the shape of the absorption and emission spectra of the biliverdin chromophore. We confirmed that the fluorescence properties of both samples are very similar *in vivo* and *in vitro*. However, we found that the paraformaldehyde fixation of the *Escherichia coli* cells containing the recombinant phytochrome protein significantly changed the fluorescence properties of the chromophore-binding domain. The biliverdin fluorescence was diminished almost completely, and the fluorescence originated only from the protoporphyrin molecules. Our results emphasize that the effect of protoporphyrin IXa should not be ignored in the fluorescence experiments with phytochrome systems while designing better red fluorescence markers for cellular imaging.

INTRODUCTION

Phytochromes are photoreceptors sensitive to the red and far-red regions of the visible light spectrum.[1,2] The photoconversion between the passive (red-light absorbing, Pr) and active (far-red-light absorbing, Pfr) states functions as a master switch in numerous signaling cascades, including seed germination, flower induction, and leaf development in plants and chromatic adaptation, circadian rhythm, phototaxis, gene expression, and carotenoid regulation in bacteria.[3−9] They were the second group of photoreceptors characterized biochemically, and their important role drives continuing interest.[10,11] In proteobacterial *Deinococcus radiodurans* (*Dr*) phytochrome, N-terminal domains PAS (**P**er/**A**rnt/**S**im) and GAF (c**G**MP phosphodiesterase/adenyl cyclase/**F**hlA) form the chromophore-binding domain (CBD) that binds linear tetrapyrrole biliverdin IX (BV) by a thioether bond to a conserved cysteine residue. The CBD is attached to a PHY (**Phy**tochrome-specific) domain, which is required for formation and stability of the Pfr state conformation.[9,12−16]

To study the mechanism of the photoconversion between the Pr and Pfr states and the intermediates formed during the conversion, low-temperature methods,[17] time-resolved optical spectroscopy,[18−20] resonance Raman spectroscopy, and other methods have been used.[21−23] Photoconversion involves several intermediates in the time scales ranging from picoseconds to milliseconds.[17,18,24] The primary step in photoconversion is a photoinduced *cis*−*trans* isomerization at the C15═C16 bond of the BV leading to a transition from the Pr to the so-called Lumi-R state.[12,22,25−27] This formation has been shown to take place within the hundreds of picoseconds time range.[18−20] Knowledge of the excited state dynamics of phytochromes is vital for understanding the early step of the photoinduced transformation from the Pr to Pfr states. In

Special Issue: Rienk van Grondelle Festschrift

Received: December 7, 2012
Revised: February 22, 2013
Published: March 6, 2013

plants and cyanobacterial systems, the chromophore is either phytochromobilin, phycocyanobilin, or phycoerythrobilin and the excited state lifetimes of the Pr state vary between 10 and 100 ps.[28,29] Such lifetimes can also be found from BV binding bacterial phytochromes, e.g., *Agrobacterium tumefaciens* (Agp1).[30] However, Kennis and co-workers have demonstrated a rather long (~300−500 ps) excited state lifetime of *Rhodopseudomonas palustris* (*Rp*) phytochrome BphP3 that was explained by unusual stabilizing interactions between protein side chains and the Pr conformation of the BV D-ring.[20] Most kinetic studies have been performed with the so-called full-length phytochrome systems, where all PAS−GAF−PHY domains are present,[18,19,30,31] and fewer spectroscopic studies have been conducted on the CBD where only PAS−GAF domains are present (i.e., *Rp*BphP2 and *Rp*BphP3 or *Dr*CBD).[31] Nevertheless, for *Dr* phytochrome, the structures of only the PAS−GAF domains are known.[12,13,32] Site-selective mutations of the *Dr*CBD can lock the photoconversion in the Pr state. One such mutation is the aspartate 207 to histidine substitution (D207H) that obstructs the progression of the photoconversion.[24,32] The histidine side chain introduced by the mutation changes the hydrogen bonding network of the binding pocket, likely unstabilizing the BV D-ring conformation required for the Pfr state and promoting a back-flip to the Pr state from the subsequent Lumi-R state.[32]

The fluorescence potential of phytochromes has been known for a long time.[5,24,33−35] Fluorescent phytochromes were first reported by Fischer and Lagarias[33] and Vierstra and co-workers.[24] In an important recent development, a near-infrared fluorescent mutant of *Dr*CBD was reported to be useful for *in vivo* imaging.[36,37] Emission at around 800 nm is of particular interest for tissue imaging, since this part of the electromagnetic spectrum is not hindered by absorption or autofluorescence from natural agents in the cellular environment and the scattering of light is diminished. The fluorescence of the natural *Dr*CBD is, however, rather weak due to its low fluorescence quantum yield[32] but has been shown to be improved by site-selective mutations of the CBD.[32] Thus, fluorescence properties of *Dr*CBD are continuously developed to produce a fluorescent marker protein that would be especially useful for live tissue imaging.[32]

To improve the fluorescence properties of the molecules, detailed knowledge of the excited state dynamics is crucial. Here, we report the excited state properties of the Pr state of *Dr*CBD and *Dr*CBD-D207H *in vitro* and *in vivo* by using steady-state and time-resolved absorption and fluorescence techniques. These studies provide information on the early phase of the Pr transition toward the Pfr state, and contribute to the development of the fluorescence properties of the construct based on *Dr*CBD molecules. In addition, we provide information about the use of these systems in cell environment and in particular report the effect of fixation, commonly used in the cell and molecular biology, on the fluorescence properties of *Dr*CBD. The effects of fixation are not extensively studied but have been shown to alter the fluorescence lifetime in certain yellow-fluorescent proteins.[38]

EXPERIMENTAL SECTION

Plasmids. Plasmid for the expression of wild-type *Dr*CBD was obtained from Prof. R. D. Vierstra's laboratory (*Dr*CBD gene in vector pET21b(+)).[12] Expression plasmids for the *Dr*CBD mutant *Dr*CBD-D207H and for the *Synechocystis* PCC6803 hemeoxygenase (Ho1) were based on the IFP1.0 plasmid obtained from the laboratory of Prof. R. Y. Tsien.[36] Standard PCR methods were used to introduce restriction sites to the ends of the D207H and Ho1 genes from the IFP1.0 plasmid. Consequently, the *Hin*dIII-XhoI restricted D207H insert was ligated to the pET21b(+) (Novagen) vector, and the NdeI-*Bam*HI restricted Ho1 was ligated to the pAP98 vector, a plasmid produced *in house* to allow dual-plasmid expression, containing p15A origin of replication, kanamycin resistance, *lacI* and *lac* operon. The individual expression plasmid for BV-producing Ho1 enabled the production of the apoprotein and holoprotein in a controlled manner. For expression, plasmids were transformed to competent *E. coli* BL21(DE3) cells (Novagen) with the heat shock method.

Protein Expression. *Dr*CBD and *Dr*CBD-D207H were expressed in strain BL21 (DE3) either by themselves or simultaneously with the Ho1. Expression cultures grown in LB medium with 150 μg/mL ampicillin (to select apoprotein plasmids) and 25 μg/mL chloramphenicol (to select the Ho1 plasmid) were incubated at +28 °C and 230 rpm until the OD_{550} reached 0.5−0.6. Cultures were induced with 1 mM IPTG and incubated overnight, after which the cells were gathered with centrifugation. Pellets were resuspended to a 1:20 ratio in (20 mM Tris, 50 mM NaCl, pH 7) storage buffer.

Protein Purification. Cells were disrupted either with French Pressure Cell (Thermo Fisher Scientific) or with bead beating using 0.1 mm glass beads (MO BIO Laboratories Inc.), using pressure for the *Dr*CBD-D207H mutant and bead beating for the more sensitive native *Dr*CBD. Insoluble impurities were separated from the rough lysate with subsequent low-speed (20 min, 7600*g*, +4 °C) and high-speed (2 h, 80000*g*, +5 °C) centrifugation steps. For the samples in the transient absorption experiments, the cleared lysate was incubated 2 h or overnight with at least 10× molar excess of BV (Frontier Scientific). The target protein was purified from the supernatant with nickel-nitrilotriacetic acid (Ni-NTA) chromatography using the HisTrap FF crude column (GE Healthcare) with the ÄKTA Prime Plus chromatography system (GE Healthcare). Impurities were removed by washing with buffer containing 130 mM imidazole and target protein eluted with 500 mM imidazole. Collected fractions were analyzed in 15% SDS-PAGE. Fractions containing the purified target protein were pooled and concentrated with the Amicon ultrafiltration system. During concentration, the sample buffer was changed to (20 mM Tris, 50 mM NaCl, pH 7). The protein concentration of the final samples was measured with the NanoDrop 1000 spectrophotometer (Thermo Fisher Scientific), and the pure dimeric nature of the proteins was ensured with analytical size exclusion chromatography (BioSep3000 column installed in the Shimadzu VP10 HPLC system). Final samples were stored at +8 °C or at −80 °C for short- or long-term storage, respectively.

Spectroscopic Measurements. The steady-state spectra of the samples were diluted in (20 mM Tris, 50 mM NaCl, pH 7) for OD_{700} of 0.1. The spectra were recorded using the Perkin-Elmer LAMBDA 850 UV−vis spectrophotometer and the Varian Cary Eclipse fluorescence spectrophotometer. Measurements were carried out under ambient conditions. The fluorescence intensities were corrected for the number of absorbed photons.

Determination of Quantum Yields. Fluorescence quantum yield measurements were performed using the Varian Cary Eclipse fluorecence spectrophotometer. The excitation wavelength was 630 nm. The excitation density was kept low to

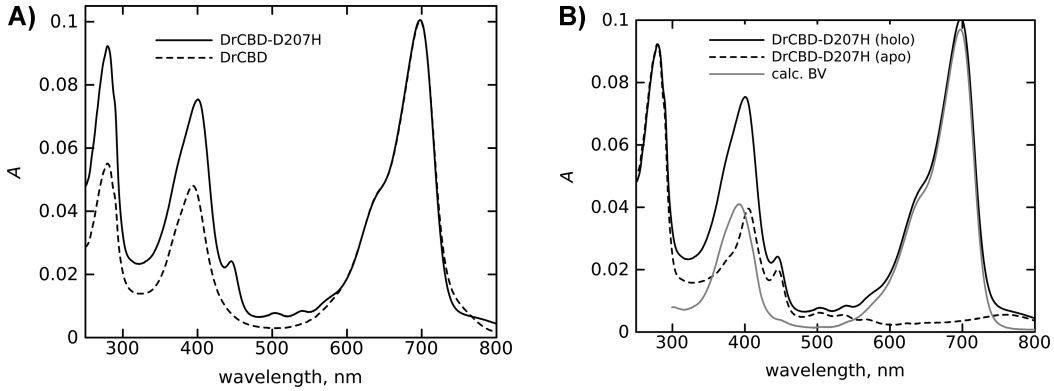

Figure 1. Absorption spectra of the purified (A) *Dr*CBD (dashed) and *Dr*CBD-D207H (solid) holoprotein and (B) *Dr*CBD-D207H apoprotein (dashed black) and holoprotein (solid black), and calculated BV absorption spectra (solid gray).

avoid photoconversion of the phytochrome samples; its absence was confirmed by the identity of absorbance spectra immediately before and after the fluorescence experiments. The quantum yields (Φ) of the D*r*CBD and D*r*CBD-D207H dissolved in (20 mM, 50 mM NaCl, pH 7.0) were determined relative to reference fluorophore with known quantum yield.[39] Cy5 (Amersham, Pittsburgh, PA) dissolved in phosphate-buffered saline (PBS) was used as a fluorescence quantum yield standard (Φ_R = 0.27).[40] The following formula was used to determine Φ:[39]

$$\Phi_F = \frac{A_R}{A_F}\frac{F_F}{F_R}\Phi_R \quad (1)$$

where Φ_F is the quantum yield to be determined, Φ_R the quantum yield of the reference, A_F the absorbance at the excitation wavelength of the dye, A_R the absorbance at the excitation wavelength of the reference dye, F_F the integrated area of the fluorescence of the dye, and F_R the integrated area of the fluorescence spectrum of the reference dye. Specifically, Φ_F was determined as follows: (1) the absorbance spectra of sample and reference were measured (the OD_{630} of the solutions was always lower than 0.1 so as to avoid an inner filter effect); (2) the emission spectra of sample and reference were recorded at the same wavelength; (3) the areas of the emission spectra were integrated.

The pump−probe technique for time-resolved absorption was used to detect fast processes with a time resolution shorter than 0.2 ps. A laser setup with an integrated one box femtosecond laser (Quantronix) was used to pump two home-built noncollinear optical parametric amplifiers (NOPAs) to produce the 680 nm pump pulses and the 760 nm probe pulses. An excitation pulse energy of about 10^{14} photons/cm^2 was used in all measurements. Further details of the experimental setup have been described by Benkö et al.[41] The transient traces were measured with and without 780 nm LED illumination, which ensured the initial population of the Pr state. However, with the present samples, no clear differences between illuminated and nonilluminated samples were observed.

Fluorescence decays of the samples in the sub-nanosecond and nanosecond time scales were measured using a time-correlated single photon counting (TCSPC) system consisting of a PicoHarp 300 controller and a PDL 800-B driver (PicoQuant GmBH). The excitation wavelengths were 405 and 650 nm from pulsed diode laser heads LDH-P-405 and LDH-P-650, respectively. The fluorescence signal was detected with a micro channel plate photomultiplier tube (Hamamatsu R3809U). The time resolution was approximately 60−70 ps (full width at half-maximum (fwhm) of the instrument response function (IRF)).

Confocal Microscopy, Sample Preparation, and Imaging. Protein expression was conducted as described earlier. After the overnight incubation of the IPTG-induced cultures, cells were gathered with centrifugation and resuspended to a 1:1 ratio in (20 mM Tris, 50 mM NaCl, pH 7) buffer. Cells were administered to the poly-L-lysine treated glass substrate and incubated for 20 min, followed by removal of the nonadherent cell suspension. For live samples, adherent cells were immobilized by the addition of liquid soft agar. For fixed samples, cells were fixed with 4% paraformaldehyde and mounted in Mowiol-Dabco media. The live and fixed samples were either imaged immediately or stored in a +8 °C cold room protected from light until imaging.

In vivo emission spectra were obtained with a Olympus FV1000 in an IX-81 inverted microscope. The 60× water (NA = 1.2) or 60× oil (NA = 1.35) objectives were used for live and fixed cell detection, respectively. Photomultiplier tubes (Hamamatsu R6357) with a flat frequency response within the scanned frequencies were used for detection. The 633 nm laser line was used for phytochrome excitation, and the emitted fluorescence was detected using a 640−800 nm bandpass filter. The slit width was adjusted according to 20 nm resolution (fwhm), and the spectra were collected with a step size of 10 nm. The scanning speed was 4 μs/pixel. The pinhole size was adjusted to 1 Airy unit. The size of the measurement area was 512 × 512 pixels^2 corresponding to the dimensions of 42 × 42 μm^2.

Fluorescence Lifetime Microscopy (FLM). Samples were prepared as described for confocal microscopy. Fluorescence lifetime images were acquired by using a fluorescence lifetime microscope MicroTime-200 (PicoQuant GmBH) coupled to the inverted microscope Olympus IX-71 (Olympus). FLM with a 100× oil objective having NA 0.8 enabled a minimum spatial resolution of 0.3 μm and a maximum scan area of 80 × 80 μm^2. The excitation wavelength was 650 nm, and the time resolution was approximately 60−70 ps (fwhm of the IRF). The SymPhoTime v. 4.7 software was used to calculate the lifetime map images.

RESULTS

Steady-State Absorption and Fluorescence. Steady-state absorption of *Dr*CBD-D207H in Figure 1A indicates that

dx.doi.org/10.1021/jp312061b | J. Phys. Chem. B 2013, 117, 11049−11057

the features of the *Dr*CBD-D207H BV Q-band, the region between 600 and 750 nm, overlap fully with the absorption spectrum of *Dr*CBD samples in its Pr state.[36,42] However, the Soret bands, in the region around 400 nm, deviate between the samples. This difference originates from binding of the other type of chromophore, most likely protoporphyrin IXa (PPIXa) molecules, in the binding pocket. This hypothesis can be confirmed by comparing the absorption spectra of purified *Dr*CBD-D207H apoprotein and holoprotein, shown in Figure 1B. The apoprotein means that the samples are grown without the Ho1 plasmid and thus do not contain any BV but only the natural amount of PPIXa molecules. In the case of the apoprotein samples, absorption of the PPIXa bound to phytochrome proteins is detected (Figure 1B). This allows the absorption spectrum of the BV chromophore to be calculated. The spectrum resembles closely that of the *Dr*CBD samples in Figure 1A. Thus, the absorption spectrum of the purified *Dr*CBD-D207H apoprotein in the blue part of the spectrum is the superposition of the absorption properties of BV and porphyrin chromophore with a maximum at 405 nm. By using the extinction coefficients of PPIXa ε_{403} = 141 000 M^{-1} cm^{-1}, *Dr*CBD-D207H ε_{700} = 92 629 M^{-1} cm^{-1}, and *Dr*CBD ε_{700} = 108 600 M^{-1} cm^{-1}, the ratios between BV and PPIXa are 0.26 and 0.02 for *Dr*CBD-D207H and *Dr*CBD, respectively.[32,43] It is also notable that illuminating the samples with 680 nm external light reveals a photoconverted absorption spectrum in the case of *Dr*CBD samples, where the 700 nm band drops by half and a band at around 750 nm increases considerably, similar to Auldridge et al.[32] (data not shown).

The fluorescence spectra of the *Dr*CBD-D207H mutant and *Dr*CBD samples, when excited at the Q-band of BV at 650 nm, are presented in Figure 2A. The obtained fluorescence emission originates naturally from the BV molecules, and the shape of the spectra remains basically the same in both samples, in line with the absorption measurements described above. The maxima of the spectra are located near 720 nm. When 405 nm excitation is used, corresponding to the Soret-band absorption, clear differences between the *Dr*CBD and *Dr*CBD-D207H samples are obtained. Much stronger fluorescence with maxima at 622 and 688 nm is observed in the case of the *Dr*CBD-D207H sample (Figure 2B) compared to the emission of the *Dr*CBD wild-type samples (Figure 2C). In addition, minor emission bands are observed around 655 nm, mainly in the case of the *Dr*CBD-D207H samples. All of these emission bands can be assigned to PPIXa fluorescence bands, which show much longer lifetimes, and therefore higher fluorescence yields than the BV molecules,[43] *vide infra*. It is likely that the 655 nm emission originates from a slightly different binding orientation of the PPIXa molecules in the binding pocket. Still, with the 405 nm excitation, both samples show BV emission at around 720 nm, in line with a previous study.[24] The fluorescence quantum yields were determined to be 0.035 ± 0.005 (*Dr*CBD) and 0.040 ± 0.005 (*Dr*CBD-D207H).

Time-Resolved Absorption and Fluorescence. The results from the time-resolved fluorescence decay measurements with the TCSPC method with excitation wavelengths of 405 and 650 nm and monitoring wavelengths of 622 and 720 nm are presented in Figure 3A and B. Evidently, the decays were not monoexponential, and several exponential decay components were needed to fit the experimental data. Typical fitting curves are shown in Figure 3, and the fit results are summarized in Table 1.

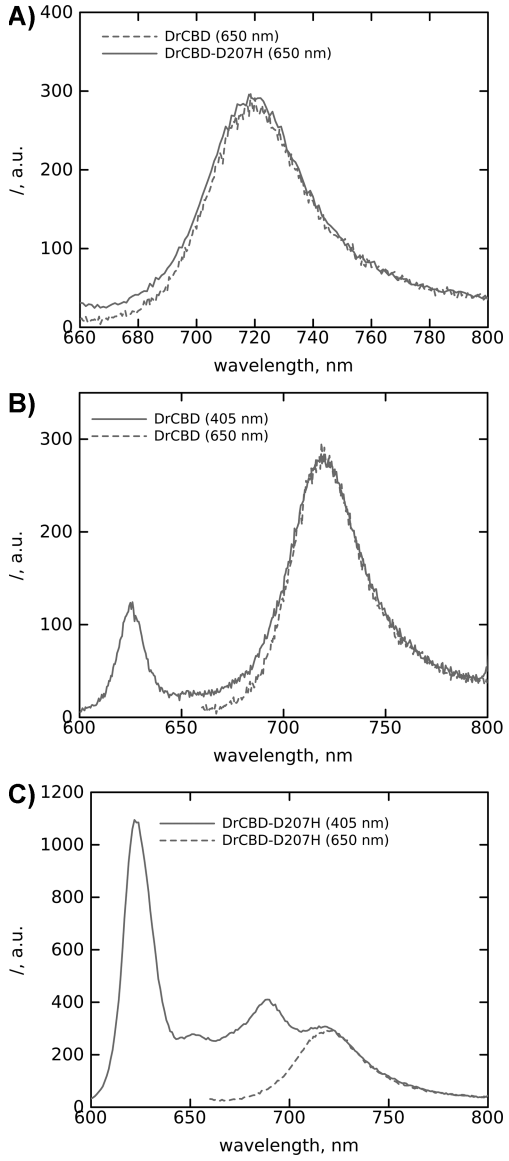

Figure 2. Steady-state emission spectra of purified (A) *Dr*CBD and *Dr*CBD-D207H proteins excited at 650 nm excitation light, (B) *Dr*CBD with excitation at 405 nm (solid gray) and 650 nm (dashed gray), and (C) *Dr*CBD-D207H with excitation at 405 nm (solid gray) and 650 nm (dashed gray). The fluorescence intensities were corrected for the number of absorbed photons.

Fluorescence decays of apoprotein samples are best described with a biexponential function with lifetimes of about 2 and 15 ns, which are attributed to the decay of PPIXa fluorescence, in line with a previous study.[44] Naturally, the fluorescence from PPIXa influences the fluorescence decay of the holoprotein samples when excited at 405 nm. In this case, we observe one fast fluorescence decay component of about 300 ps and two longer components. The first component can be assigned purely to the decay of the BV, the second one is a mixture of the BV and PPIXa fluorescence decay, and the final 10 ns component originates purely from the PPIXa molecules. Similarly to the steady-state measurements, one can observe a larger number of PPIXa molecules in the *Dr*CBD-D207H samples than in the wild-type *Dr*CBD samples.

With excitation at 650 nm and monitoring at 720 nm, the excitation decay properties of BV molecules in the binding

dx.doi.org/10.1021/jp312061b | J. Phys. Chem. B 2013, 117, 11049−11057

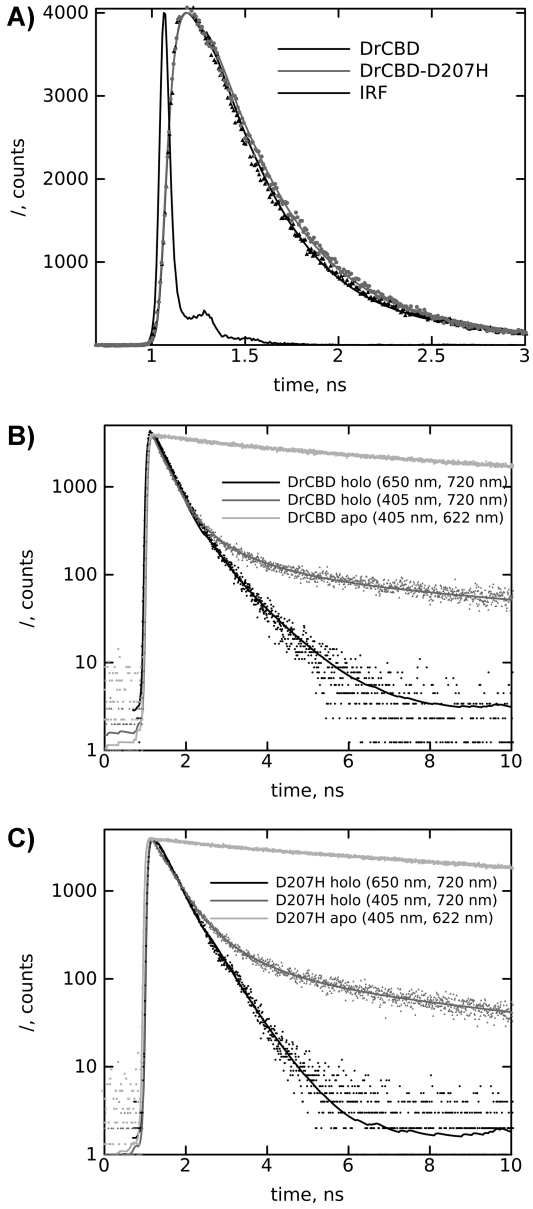

Figure 3. Emission decays of purified (A) *Dr*CBD and *Dr*CBD-D207H proteins excited at 650 nm and monitored at 720 nm. IRF is the instrument response function. Emission decays of purified (B) wild-type *Dr*CBD and (C) *Dr*CBD-D207H excited at 405 and 650 nm and monitored at 622 and 720 nm. Solid lines show the multiexponential fit of the data.

pocket can be studied. In both studied samples, the fluorescence decay can be fitted biexponentially. In Figure 3A, one can observe slight differences in the decay profiles, although the average fluorescence lifetimes are about 370 ps in both samples. These small differences in decay indicate the effect of the aspartic acid, replaced by histidine in the mutant, on the excited state decay of the BV in the binding pocket. The fluorescence measurements, thus, indicate somewhat faster decay in the subnanosecond range in the case of *Dr*CBD than in the case of the *Dr*CBD-D207H mutant. This was studied in more detail, using the time-resolved absorption technique. By exciting with a 680 nm laser pulse and detecting at 760 nm, the decay of the stimulated emission can be observed for the BV, and hence the excited state decay. The transient absorption traces, shown in Figure 4, again exhibit nonexponential decay

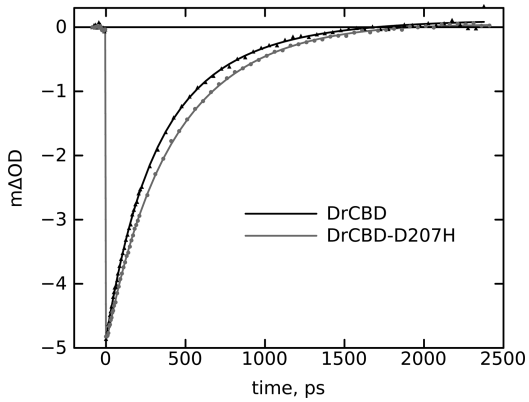

Figure 4. Transition absorption decay traces of *Dr*CBD and its *Dr*CBD-D207H mutant excited at 680 nm and monitored at 760 nm. Solid lines show the multiexponential fit of the data.

kinetics, and similar to the fluorescence kinetics, the transient absorption kinetics of *Dr*CBD and *Dr*CBD-D207H are slightly different. In the early phase of the data, a fast 5 ps (rise) dynamic is observed. Then, the excited state decay can be described by the triexponential components, with time constants of about 240 ps, 610 ps, and 1 ns for *Dr*CBD-D207H and 240 ps, 560 ps, and about 3 ns for the *Dr*CBD samples.

Confocal and Fluorescence Lifetime Microscopies. Above we have described in detail the excited state properties of BV and PPIXa molecules in CBD and the mutant *Dr*CBD-D207H *in vitro*. We also wanted to verify how these properties are retained in the cellular environment. Figure 5 shows the fluorescence spectra of the *Dr*CBD and *Dr*CBD-D207H

Table 1. Results of the Fluorescence Decay Fits[a]

sample	τ_1 (ps)	τ_2 (ns)	τ_3 (ns)
*Dr*CBD-D207H hp (650 nm, 720 nm)	240 ± 30 (64%)	0.61 ± 0.03 (36%)	
*Dr*CBD-D207H hp (405 nm, 720 nm)	380 ± 30 (85%)	1.1 ± 0.2 (13%)	9.0 ± 0.6 (2%)
*Dr*CBD-D207H ap (405 nm, 622 nm)		2.1 ± 0.4 (87%)	15.2 ± 0.2 (13%)
*Dr*CBD hp (650 nm, 720 nm)	306 ± 15 (89%)	0.93 ± 0.07 (11%)	
*Dr*CBD hp (405 nm, 720 nm)	314 ± 20 (91%)	1.3 ± 0.3 (7%)	11.9 ± 1.0 (2%)
*Dr*CBD ap (405 nm, 622 nm)		2.5 ± 0.3 (81%)	15.3 ± 0.2 (19%)

[a] τ_1, τ_2, and τ_3 are the lifetimes, and the percentage indicates the relative amplitude of each lifetime to the overall decay curve. The weighted mean square deviations (the χ^2 value), providing information about the goodness of the fit, stayed in all cases in the range from 1.06 to 1.16. The error margins are the results of fitting. In addition to three components mentioned in the table, a fast rise component of about 30 ps was needed for the fit, which is in the limit of the time resolution of the experiment and is omitted from the table.

dx.doi.org/10.1021/jp312061b | J. Phys. Chem. B 2013, 117, 11049−11057

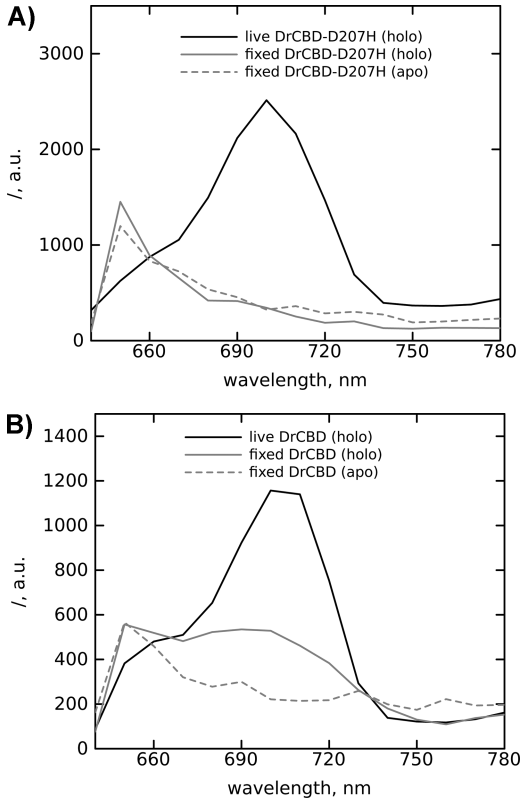

Figure 5. Emission spectra of (A) *Dr*CBD-D207H mutant and (B) *Dr*CBD in *E. coli* live (solid black) and fixed (solid gray) cell samples on a glass substrate. Fixed apoprotein emission is also shown (dashed gray). The excitation wavelength was 633 nm.

proteins in live or fixed cells. In the same figure, PPIXa emission spectra are also shown, which were detected by measuring the apoprotein constructs in the live and fixed cell formulations. The fluorescence spectra of the *Dr*CBD-D207H mutant and the *Dr*CBD holoprotein in the live cell samples show only one band at ca. 715 nm. These bands can be identified to the BV emission (Figure 2). Fixation shifts the fluorescence maximum to blue in both samples, though *Dr*CBD holoprotein still shows some emission between 670 and 720 nm. Similarly to the *in vitro* experiments, the study of apoprotein reveals information about the emission spectra of the PPIXa molecules in the binding pocket. The apoprotein from both constructs shows spectra with the strongest peak at 650 nm followed by some bands at the longer wavelengths, similarly to the steady-state emission data in Figure 2. Naturally, the emission band at 622 nm, observed in the steady-state emission curves, is missing, as we used the 633 nm excitation wavelength in our *in vivo* experiments.

Fluorescence lifetime microscopy (FLM) measurements were performed for live and fixed cell samples deposited on glass substrates. Figure 6 presents the FLM images of *Dr*CBD-D207H in live and fixed cell samples. In live cells expressing *Dr*CBD-D207H, the fluorescence was evenly distributed throughout the cytoplasm. The average lifetimes were clearly in line with the *in vitro* experiments, being less than 1 ns. However, the FLM images of *Dr*CBD-D207H in the fixed cells show many more irregularities in terms of lifetimes, as presented in Figure 6B. The average lifetime increases considerably, being greater than 4 ns in some parts of the cells. Notably, the *Dr*CBD reveals very similar data with the

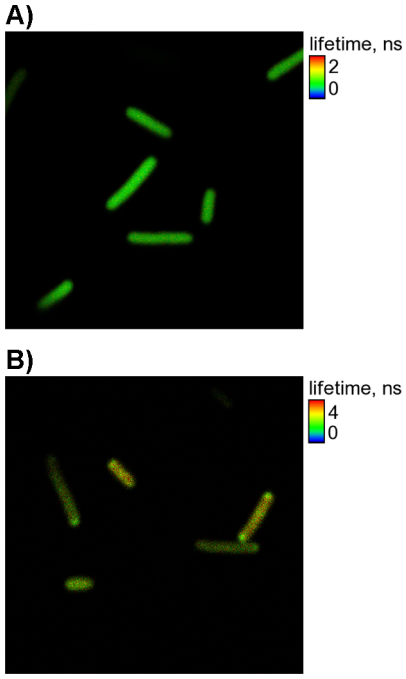

Figure 6. FLM image of *Dr*CBD-D207H in *E. coli* (A) live and (B) fixed cell samples on a glass substrate. The excitation wavelength was 650 nm. The scan sizes are 15 μm.

*Dr*CBD-D207H mutant (data not shown), whereas the effect of the fixation on the lifetimes is stronger in the case of the *Dr*CBD-D207H mutants.

FLM allowed us to calculate the emission decays for cells. In these measurements, the rise of the fluorescence decay several tens of picoseconds were omitted, because IRF was not measured. Figure 7A presents the averaged emission decay curves of the *Dr*CBD-D207H mutant in cells. In live cells, i.e., in the absence of fixation, the average lifetime is about 0.5 ns, comparable to those measured *in vitro* (Table 1). However, the average fluorescence lifetime is increased to about 2.2 ns upon fixation of the cells, which resembles the lifetime of the PPIXa molecules, measured *in vitro* (Table 1). In addition, Figure 7B indicates that the distribution of the fluorescence lifetimes is much narrower in the case of live cell detection compared with fixed cell detection.

■ DISCUSSION

Our studies focused on the excited state properties of the CBD truncations of the *Deinococcus radiodurans* phytochrome. *Dr*CBD, truncated at residue 321, lacks the PHY domain and thus is unable to complete the photoconversion observed in full-length proteins.[12,24] In addition, we studied a *Dr*CBD-D207H mutant that is considered to be "locked" in the Pr state.

Similar to previous time-resolved studies of phytochrome systems,[20,28−30] we analyzed the time-resolved fluorescence and transient absorption data using a multiexponential decay fit. Since only single-wavelength measurements were carried out in this study, any discussion of a particular reaction scheme for the excited state Pr to thr Lumi-R-state is beyond the scope of this paper. Nevertheless, the exponential decay analysis allows us to determine the average decay times for the *Dr*CBD and *Dr*CBD-D207H samples to be about 370 ps in both experiments. When compared with excited state lifetimes of chromophore-binding domains from R*p*BphP2 and R*p*BphP3 samples, the 370 ps

dx.doi.org/10.1021/jp312061b | J. Phys. Chem. B 2013, 117, 11049−11057

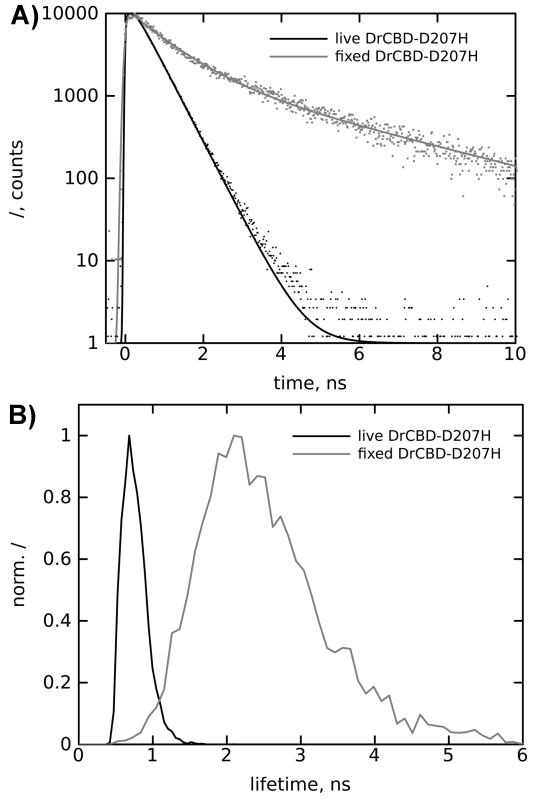

Figure 7. (A) Fluorescence decays of the *Dr*CBD-D207H mutant measured with FLM. The averaging was taken from five cells. Solid lines show an exponential fit of the data. (B) Distributions of average lifetimes for *Dr*CBD-D207H in live (black) and fixed (gray) cell samples. The samples were excited at 650 nm.

average lifetime of the D*r*CBD is actually more similar to the 382 ps fluorescence lifetime of the PAS−GAF CBD from R*p*BphP3 than that of R*p*BphP2, being of about 190 ps.[31] Moreover, in PAS−GAF CBD from R*p*BphP2 there exists a decay component of about 75 ps which is absent in *Dr*CBD samples. The R*p*BphP3 is a nonclassical phytochrome that forms a near-red light absorbing state at 645 nm, instead of the classical Pfr-state,[7] but it can be reverted to classical phytochrome function via L207Y mutation and it is structurally very similar with R*p*BphP2.[45,46] Toh et al. proposed that the longer lifetime of R*p*BphP3[46] is caused by hydrogen bonds that residues L183, H299, and S297 form with the ring D of the BV.[31] However, two residues in analogous positions in D*r*CDB[13] (M174, A288) do not form hydrogen bonds with the D-ring. In *Dr*CBD,[13] the most prominent hydrogen bonding partner to the D-ring is H290, analogous to H299 in R*p*BphP3.[46] This conserved histidine is also present in other related proteins such as cyanobacterial phytochrome Cph1.[2] The R*p*BphP3[46] structure lacks the water typically coordinated between BV pyrrole rings and conserved aspartate (D207 in *Dr*CBD[13] and Cph1[2] D216 in R*p*BphP3[46]) and is considered important for the proton transfer during BV photoconversion. However, there is also another conserved water close to the D-ring present in all phytochrome structures including R*p*BphP3. Thus, the explanation of the differences in excited state lifetime between these species at the molecular level remains unclear.[20,30]

Samma et al. have shown in their simulations that the excited state of *Dr*CBD-D207H has a slightly restricted dihedral space compared to the wild-type structure,[47] although the structures of *Dr*CBD[13] and *Dr*CBD-D207H[32] show practically no other structural differences in the binding pocket than the D207H substitution.[32] Our experiments showed, however, slight changes in the excited state kinetic profiles. Whether the small changes in the decay profiles are due to impaired Lumi-R production, impaired excited state proton transfer, or the restriction of the dihedral angle of the D-ring of the BV remains to be shown in future studies. In this study, the fluorescence yields and the average excited state decay times of the BV remain similar in both samples. This seems to be somewhat of a contradiction to the observations of Auldridge et al.,[32] who reported the quantum yield was about 50% higher in the case of the D207H mutant. The difference between our and their experiments is that our measurements are in cuvettes with volumes of about 1 mL, whereas Auldridge et al.[32] performed the fluorescence experiments by using micro channel plate readers. In the latter case, the photo production of the *Dr*CBD samples may lead to lowering of the amount of excited molecules by the 690 nm light used in their experiments, leading to lower quantum yields.[32] Thus, the quantum yield of 0.035, observed for *Dr*CBD, remains a more realistic value. The fluorescence quantum yield Φ_F is related to the fluorescence lifetime τ_F (i.e., the excited-state lifetime) and radiative time constant τ_R through the relation $\tau_F = \Phi_F\tau_R$. With the average excited-state lifetime of about 370 ps and the quantum yield of 0.035, we obtain the radiative time constant of about 10.5 ns for the *Dr*CBD systems, which is in reasonable agreement with the value found by Toh et al. for phytochrome systems in *Rh. Palustris*.[31]

The clearest difference between *Dr*CBD and *Dr*CBD-D207H is the stronger PPIXa binding in the case of the D207H mutant, which applies in our dual-plasmid system and when the apoprotein are expressed in *E. coli* without BV. This observation is in line with previous studies.[24,32] The folding of *Dr*CBD[13] and *Dr*CBD-D207H[32] is nearly identical, and binding pockets of the structures even have most structural waters at similar positions.[32] Hence, we can only speculate that the positively charged mutated H207 facilitates whereas the wild-type D207 hinders the binding of the PPIXa molecules into the CBD binding pocket. The higher number of PPIXa molecules affects the fluorescence properties of the phytochrome systems if blue light (below 600 nm) is used for the excitation. Hence, this effect needs to be taken into account when using for example dual excitation procedures with phytochrome-based fluorescence markers for cell imaging purposes.

Although the fluorescence properties of the BV molecules in live cell imaging remain similar to those observed *in vitro*, the paraformaldehyde fixation of phytochrome CBDs causes clear changes in the fluorescence properties of the *Dr*CBD systems, in terms of spectral and lifetime behavior of the molecules. The blue-shifted emission observed in the fixed *Dr*CBD-D207H and *Dr*CBD is caused by the cellular PPIXa molecule. In the fixed *Dr*CBD-D207H, emission from the BV disappears virtually completely, leaving only the porphyrin emission in this spectral range. This signal, however, shows a much broader lifetime distribution, indicating a very heterogeneous environment around the PPIXa molecules. The paraformaldehyde fixation causes methylene bridges to form between a nitrogen atom at the end of the side-chain of a lysine and the nitrogen atom of a peptide linkage in the vicinity. In *Dr*CBD, aspartate 207 has a negative side chain positioned close to the BV D-ring and likely

dx.doi.org/10.1021/jp312061b | *J. Phys. Chem. B* 2013, 117, 11049−11057

participates in forming the hydrogen bond network that enables the photoconversion. In the *Dr*CBD-D207H mutant, the negative side chain is substituted with a positive, creating conditions potentially more attractive to the fixation agent. In *Dr*CBD, the negative aspartate side-chain is less likely to participate in fixation, and some of the BV emission is retained.

CONCLUSIONS

In this study, we have shown that the average excited state lifetime of BV in *Dr*CBD is ca. 370 ps, which is similar to the one observed for *Rp*BphP3 molecules.[20,31] The D207H mutation slightly increases the excited state lifetime of the system, albeit the mutation does not affect the shape of the absorption or emission spectra of the BV in the binding pocket. Even though there are some deviations in the amino acid residues in the binding pocket, the excited state lifetime properties of *Dr*CBD are quite similar to those of the *Rp*BPhP3,[46] observed by Toh et al.[20,31] This indicates that understanding of the role of the amino acid network around the BV molecules in the phytochrome systems is still sparse. We have also shown that the D207H mutation in a crucial position in the binding pocket affects to some extent the kinetics of the excited state of the BV, but the average lifetime and the fluorescence yield of the BV remain practically unchanged. In addition, our study shows that there are factors that can cause difficulties for using phytochrome-based fluorescent markers for cell imaging when fixation is used. We stress that the binding of the heme molecules to the CBD must always be considered, and fixation agents may cause considerable changes in the fluorescence properties of the BV phytochromes.

AUTHOR INFORMATION

Corresponding Author

*E-mail: janne.ihalainen@jyu.fi.

Notes

The authors declare no competing financial interest.

ACKNOWLEDGMENTS

Authors thank Prof. R. D. Vierstra and Prof. R. Tsien for providing the expression plasmids for *Dr*CBD and IFP1.0, respectively. A. Pawlowski is acknowledged for providing the pAP98 plasmid, Eila Korhonen and Alli Liukkonen for help with purification of the proteins, Jenni Karttunen for help in cell fixation procedure, and Dr. Pasi Myllyperkiö for helping in the laser laboratory. The research was supported by the Academy of Finland (SA grants 138063, 251106, and 1129648). Structure Figure was generated using Pymol (Delano Scientific, San Carlos, http://pymol.sourceforge.net/) and atomic coordinates with PDB ID: 3S7N).[32]

REFERENCES

(1) Quail, P. H. A lIght-Sensing Knot Revealed by the Structure of the Chromophore-Binding Domain of Phytochrome. *Nat. Rev. Mol. Cell Biol.* **2002**, *3*, 85−93.

(2) Essen, L. O.; Mailliet, J.; Hughes, J. The Structure of a Complete Phytochrome Sensory Module in the Pr Ground State. *Proc. Natl. Acad. Sci. U.S.A.* **2008**, *105*, 14709−14714.

(3) Kehoe, D. M.; Grossman, A. R. Similarity of a Chromatic Adaptation Sensor to Phytochrome and Ethylene Receptors. *Science* **1996**, *273*, 1409−1412.

(4) Schmitz, O.; Katayama, M.; Williams, S. B.; Kondo, T.; Golden, S. S. CikA, a Bacteriophytochrome That Resets the Cyanobacterial Circadian Clock. *Science* **2000**, *289*, 765−768.

(5) Giraud, E.; Fardoux, J.; Fourrier, N.; Hannibal, L.; Genty, B.; Bouyer, P.; Dreyfus, B.; Verméglio, A. Phytochrome Controls the Photosystem Synthesis in Anoxygenic Bacteria. *Nature* **2002**, *417*, 202−205.

(6) Yoshihara, S.; Suzuki, F.; Fujita, H.; Geng, X. X.; Ikeuchi, M. Novel Putative Photoreceptor and Regulatory Genes Required for the Positive Phototactic Movement of the Unicellular Motile Cyanobacterium Synechocystis. *Plant Cell Physiol.* **2000**, *41*, 1299−1304.

(7) Giraud, E.; Zappa, S.; Vuillet, L.; Adriano, J.-M.; Hannibal, L.; Fardoux, J.; Berthomieu, C.; Bouyer, P.; Pignol, D.; Verméglio, A. A New Type of Bacteriophytochrome Acts in Tandem with a Classical Bacteriophytochrome to Control the Antennae Synthesis in *Rhodopseudomonas palustris*. *J. Biol. Chem.* **2005**, *280*, 32389−32397.

(8) Bhoo, S.-H.; Davis, S. J.; Walker, J.; Karniol, B.; Vierstra, R. D. Bacteriophytochromes Are Photochromic Histidine Kinases Using a Biliverdin Chromophore. *Nature* **2001**, *414*, 776−779.

(9) Davis, S. J.; Vener, A. V.; Vierstra, R. D. Bacteriophytochromes: Phytochrome-Like Photoreceptors from Nonphotosynthetic Eubacteria. *Science* **1999**, *286*, 2517−2520.

(10) Butler, W. L.; Norris, K. H.; Siegelman, H. W.; Hendricks, S. B. Detection, Assay, and Preliminary Purification of the Pigment Controlling Photoresponsive Development of Plants. *Proc. Natl. Acad. Sci. U.S.A.* **1959**, *45*, 1703−1708.

(11) Rockwell, N. C.; Lagarias, J. C. A Brief History of Phytochromes. *ChemPhysChem* **2010**, *11*, 1172−1180.

(12) Wagner, J. R.; Brunzelle, J. S.; Forest, K. T.; Vierstra, R. D. A Light-Sensing Knot Revealed by the Structure of the Chromophore-Binding Domain of Phytochrome. *Nature* **2005**, *438*, 325−331.

(13) Wagner, J. R.; Zhang, J.; Brunzelle, J. S.; Vierstra, R. D.; Forest, K. T. High Resolution Structure of Deinococcus Bacteriophytochrome Yields New Insights into Phytochrome Architecture and Evolution. *J. Biol. Chem.* **2007**, *282*, 12298−12309.

(14) van Thor, J. J.; Ronayne, K. L.; Towrie, M. Formation of the Early Photoproduct Lumi-R of Cyanobacterial Phytochrome Cph1 Observed by Ultrafast Mid-Infrared Spectroscopy. *J. Am. Chem. Soc.* **2007**, *129*, 126−132.

(15) Yang, Y.; Linke, M.; von Haimberger, T.; Hahn, J.; Matute, R.; González, L.; Schmieder, P.; Heyne, K. Real-Time Tracking of Phytochrome's Orientational Changes during Pr Photoisomerization. *J. Am. Chem. Soc.* **2012**, *134*, 1408−1411.

(16) von Stetten, D.; Seibeck, S.; Michael, N.; Scheerer, P.; Mroginski, M. A.; Murgida, D. H.; Krauss, N.; Heyn, M. P.; Hildebrandt, P.; Borucki, B.; et al. Highly Conserved Residues Asp-197 and His-250 in Agp1 Phytochrome Control the Proton Affinity of the Chromophore and Pfr Formation. *J. Biol. Chem.* **2007**, *282*, 2116−2123.

(17) Eilfeld, P.; Rüdiger, W. Absoprtion Spectra of Phytochrome Intermediates. *Z. Naturforsch., C* **1985**, *40*, 109−114.

(18) Andel, F.; Hasson, K. C.; Gai, F.; Anfinrud, P. A.; Mathies, R. A. Femtosecond Time-Resolved Spectroscopy of the Primary Photochemistry of Phytochrome. *Biospectroscopy* **1997**, *3*, 421−433.

(19) Bischoff, M.; Hermann, G.; Rentsch, S.; Strehlow, D. First Steps in the Phytochrome Phototransformation - a Comparative Femtosecond Study on the Forward ($P_r \rightarrow P_{fr}$) and Back Reaction ($P_{fr} \rightarrow P_r$). *Biochemistry* **2001**, *40*, 181−186.

(20) Toh, K. C.; Stojković, E. A.; van Stokkum, I. H.; Moffat, K.; Kennis, J. T. Proton-Transfer and Hydrogen-Bond Interactions Determine Fluorescence Quantum Yield and Photochemical Efficiency of Bacteriophytochrome. *Proc. Natl. Acad. Sci. U.S.A.* **2010**, *107*, 9170−9175.

(21) Andel, F.; Lagarias, J. C.; Mathies, R. A. Resonance Raman Analysis of Chromophore Structure in the Lumi-R Photoproduct of Phytochrome. *Biochemistry* **1996**, *35*, 15997−16008.

(22) Mroginski, M. A.; Murgida, D. H.; Hildebrandt, P. The Chromophore Structural Changes during the Photocycle of Phytochrome: A Combined Resonance Raman and Quantum Chemical Approach. *Acc. Chem. Res.* **2007**, *40*, 258−266.

(23) Ulijasz, A. T.; Cornilescu, G.; Cornilescu, C. C.; Zhang, J.; Rivera, M.; Markley, J. L.; Vierstra, R. D. Structural Basis for the

Photoconversion of a Phytochrome to the Activated Pfr Form. *Nature* **2010**, *463*, 250−254.
(24) Wagner, J. R.; Zhang, J.; von Stetten, D.; Günther, M.; Murgida, D. H.; Mroginski, M. A.; Walker, J. M.; Forest, K. T.; Hildebrandt, P.; Vierstra, R. D. Mutational Analysis of *Deinococcus radiodurans* Bacteriophytochrome Reveals Key Amino Acids Necessary for the Photochromicity and Proton Exchange Cycle of Phytochromes. *J. Biol. Chem.* **2008**, *40*, 12212−12226.
(25) Yang, X.; Kuk, J.; Moffat, K. Crystal Structure of *Pseudomonas aeruginosa* Bacteriophytochrome: Photoconversion and Signal Transduction. *Proc. Natl. Acad. Sci. U.S.A.* **2008**, *105*, 14715−14720.
(26) Yang, X.; Ren, Z.; Kuk, J.; Moffat, K. Temperature-Scan Cryocrystallography Reveals Reaction Intermediates in Bacteriophytochrome. *Nature* **2011**, *201*, 428−433.
(27) Rohmer, T.; Lang, C.; Hughes, J.; Essen, L. O.; Gartner, W.; Matysik, J. Light-Induced Chromophore Activity and Signal Transduction in Phytochromes Observed by ^{13}C and ^{15}N Magic-Angle Spinning NMR. *Proc. Natl. Acad. Sci. U.S.A.* **2008**, *201*, 15229−15234.
(28) Holzwarth, A. R.; Venuti, E.; Braslavsky, S. E.; Schaffner, K. The Phototransformation Process in Phytochrome. I. Ultrafast Fluorescence Component and Kinetic Models for the Initial $P_r \rightarrow P_{fr}$ Transformation Steps in Native Phytochrome. *Biochim. Biophys. Acta* **1992**, *1140*, 59−68.
(29) Heyne, K.; Herbst, J.; Stehlik, D.; Esteban, B.; Lamparter, T.; Hughes, J.; Diller, R. Ultrafast Dynamics of Phytochrome from the Cyanobacterium Synechocystis, Reconstituted with Phycocyanobilin and Phycoerythrobilin. *Biophys. J.* **2002**, *82*, 1004−1016.
(30) Schumann, C.; Groß, R.; Michael, N.; Lamparter, T.; Diller, R. Sub-Picosecond Mid-Infrared Spectroscopy of Phytochrome Agp1 from Agrobacterium tumefaciens. *ChemPhysChem* **2007**, *8*, 1657−1663.
(31) Toh, K. C.; Stojković, E. A.; van Stokkum, I. H.; Moffat, K.; Kennis, J. T. Fluorescence Quantum Yield and Photochemistry of Bacteriophytochrome Constructs. *Phys. Chem. Chem. Phys.* **2011**, *13*, 11985−11997.
(32) Auldridge, M. E.; Satyshur, K. A.; Anstrom, D. M.; Forest, K. T. Structure-Guided Engineering Enhances a Phytochrome-Based Infrared Fluorescent Protein. *J. Biol. Chem.* **2012**, *287*, 7000−7009.
(33) Fischer, A. J.; Lagarias, J. C. Harnessing Phytochrome's Glowing Potential. *Proc. Natl. Acad. Sci. U.S.A.* **2004**, *101*, 17334−17339.
(34) Li, L.; Murphy, J. T.; Lagarias, J. C. Continuous Fluorescence Assay of Phytochrome Assembly in Vitro. *Biochemistry* **1995**, *34*, 7923−7930.
(35) Zhang, J.; Wu, X.-J.; Wang, Z.-B.; Chen, Y.; Wang, X.; Zhou, M.; Scheer, H.; Zhao, K.-H. Fused-Gene Approach to Photoswitchable and Fluorescent Biliproteins. *Angew. Chem., Int. Ed.* **2010**, *49*, 5456−5458.
(36) Shu, X.; Royant, A.; Lin, M. Z.; Aguilera, T. A.; Lev-Ram, V.; Steinbach, P. A.; Tsien, R. Y. Mammalian Expression of Infrared Fluorescent Proteins Engineered from a Bacterial Phytochrome. *Science* **2009**, *324*, 804−807.
(37) Filonov, G. S.; Piatkevich, K. D.; Ting, L. M.; Zhang, J.; Kim, K.; Verkhusha, V. V. Bright and Stable near-Infrared Fluorescent Protein for *in Vivo* Imaging. *Nat. Biotechnol.* **2011**, *29*, 757−761.
(38) Ganguly, S.; Clayton, A. H.; Chattopadhyay, A. Fixation Alters Fluorescence Lifetime and Anisotropy of Cells Expressing EYFP-Tagged Serotonin$_{1A}$ Receptor Biochem. *Biophys. Res. Commun.* **2011**, *405*, 234−237.
(39) Mujumdar, R. B.; Ernst, L. A.; Mujumdar, S. R.; Lewis, C. J.; Waggoner, A. S. Cyanine Dye Labeling Reagents: Sulfoindocyanine Succinimidyl Esters. *Bioconjugate Chem.* **1993**, *4*, 105−111.
(40) Eaton, D. F. Reference Materials for Fluorescence Measurement. *Pure Appl. Chem.* **1988**, *60*, 1107−1114.
(41) Benkö, G.; Kallioinen, J.; Korppi-Tommola, J. E.; Yartsev, A. P.; Sundström, V. Photoinduced Ultrafast Dye-to-Semiconductor Electron Injection from Nonthermalized and Thermalized Donor States. *J. Am. Chem. Soc.* **2002**, *124*, 489−493.
(42) Lim, C. K.; Razzaque, M. A.; Luo, J.; Farmer, P. B. Isolation and Characterization of Protoporphyrin Glycoconjugates from Rat Harderian Gland by HPLC, Capillary Electrophoresis and HPLC/Electrospray Ionization MS. *Biochem. J.* **2000**, *347*, 757−761.
(43) Leonard, J. J.; Yonetani, T.; Callis, J. B. A Fluorescence Study of Hybrid Hemoglobins Containing Free Base and Zinc Protoporphyrin IX. *Biochemistry* **1974**, *13*, 1460−1464.
(44) Brancaleon, L.; Magennis, S. W.; Samuel, I. D. W.; Namdas, E.; Lesar, A.; Moseley, H. Characterization of the Photoproducts of Protoporphyrin IX Bound to Human Serum Albumin and Immunoglobulin G. *Biophys. Chem.* **2004**, *109*, 351−360.
(45) Bellini, D.; Pariz, M. Z. Dimerization Properties of the R*p*BphP2 Chromophore-Binding Domain Crystallized by Homologue-Directed Mutagenesis. *Acta Crystallogr.* **2012**, *D68*, 1058−1066.
(46) Yang, X.; Stojković, E. A.; Kuk, J.; Moffat, K. Crystal Structure of the Chromophore Binding Domain of an Unusual Bacteriophytochrome, R*p*BphP3, Reveals Residues That Modulate Photoconversion. *Proc. Natl. Acad. Sci. U.S.A.* **2007**, *104*, 12571−12576.
(47) Samma, A. A.; Johnson, C. K.; Song, S.; Alvarez, S.; Zimmer, M. On the Origin of Fluorescence in Bacteriophytochrome Infrared Fluorescent Proteins. *J. Phys. Chem. B* **2010**, *114*, 15362−15369.